Dynamic light scattering and atomic force microscopy imaging on fragments of β-connectin from human cardiac muscle

S. Marchetti,[1,2] F. Sbrana,[1,3] R. Raccis,[1] L. Lanzi,[1] C. M. C. Gambi,[1,2] M. Vassalli,[3,4] B. Tiribilli,[3,4] A. Pacini,[5] and A. Toscano[5]

[1]*Department of Physics and CNISM, University of Florence, Via G. Sansone 1, 50019 Sesto Fiorentino, Florence, Italy*

[2]*CRS–Soft Matter (CNR-INFM), Università di Roma "La Sapienza," p. A. Moro 2, 00185 Rome, Italy*

[3]*CSDC, Department of Physics, University of Florence, Florence, Italy*

[4]*Complex System Institute of the National Research Council (ISC-CNR), Florence, Italy*

[5]*Department of Anatomy, Histology, and Forensic Medicine, University of Florence, Florence, Italy*

(Received 27 July 2007; revised manuscript received 20 December 2007; published 14 February 2008)

In order to investigate the protein folding-unfolding process, dynamic light scattering (DLS) and atomic force microscopy (AFM) imaging were used to study two fragments of the muscle cardiac protein β-connectin, also known as titin. Both fragments belong to the *I* band of the sarcomer, and they are composed of four domains from I_{27} to I_{30} (tetramer) and eight domains from I_{27} to I_{34} (octamer). DLS measurements provide the size of both fragments as a function of temperature from 20 up to 86 °C, and show a thermal denaturation due to temperature increase. AFM imaging of both fragments in the native state reveals a homogeneous and uniform distribution of comparable structures. The DLS and AFM techniques turn out to be complementary for size measurements of the fragments and fragment aggregates. An unexpected result is that the octamer folds into a smaller structure than the tetramer and the unfolded octamer is also smaller than the unfolded tetramer. This feature seems related to the significance of the hydrophobic interactions between domains of the fragment. The longer the fragment, the more easily the hydrophobic parts of the domains interact with each other. The fragment aggregation behavior, in particular conditions, is also revealed by both DLS and AFM as a process that is parallel to the folding-unfolding transition.

DOI: 10.1103/PhysRevE.77.021910 PACS number(s): 87.16.Nn, 87.64.Cc, 87.64.Dz, 87.15.N−

I. INTRODUCTION

The conformation of the native structure of small proteins plays a critical role in determining their biological functions. In order to carry out its biological function properly, a protein must assume a shape, assembling into an ordered structure or folded state. The process of protein folding is driven by several factors, and the supramolecular organization of the polypeptide chains involves a complex molecular recognition phenomenon that depends on the cooperative action of weak noncovalent interactions.

Hydrogen bonding stabilizes the secondary structure, but the tertiary and quaternary structures are sometimes governed by even weaker interactions. The understanding of the role of these intermolecular interactions in protein folding and unfolding and in formation of protein aggregation is of interest in itself and is a challenge for modern research in several fields, e.g., physics, chemistry, biology, etc. An example is the development of new therapeutic strategies for the treatment and prevention of human disease associated with the failure of a protein to fold correctly, such as Parkinson's and Alzheimer's diseases, in which deposition of aggregated proteins in a variety of organs and tissues is involved. So in this paper we deal with the protein folding-unfolding process of a muscle protein, β-connectin, from the point of view of the physical and biological aspects.

A wealth of literature has demonstrated that vertebrate striated muscles contain a sarcomeric filament system made up of giant proteins, the β-connectins [1,2]. β-connectin, also called titin, is a large filamentous protein with molecular mass 3 MDa, length 900 nm, and diameter 4 nm [3,4], and is composed of elastic (*I* band) and inelastic (*A* band) parts. Despite its immense size, the secondary and tertiary structures of the molecule are relatively simple: more than 90% consists of domains similar to immunoglobulin (Ig) and fibronectin (Fn), with the structure of β sheets. The most interesting properties of β-connectin are the elastic behavior and the ability to act as a molecular spring. The flexibility and extensibility of β-connectin have been studied previously using dynamic light scattering (DLS) [4], atomic force microscopy (AFM) [5], optical tweezers [6], and transmission electron microscopy [7]. From these studies, β-connectin in solution behaves as a Gaussian coil.

Despite the abundant papers on the mechanical properties of Ig domains from *I*-band β-connectin in response to pulling forces [5,8–11], the supra-arrangement of domains along the filament and their structure and dynamics remain poorly characterized. In fact, to date, only atomic models of the single domains from the titin *I* band, I_1 [12] and I_{27} [13], respectively, are available. As is characteristic of the members of the immunoglobulin superfamily [14,15], each Ig domain folds into a β sandwich, containing eight β sheets, and can be considered an ellipsoid of 4.3-nm-long axis and equal shorter axes of 2.1 nm as reported in the Protein Data Bank [13]. Similarly, a combination of small-angle x-ray scattering (SAXS) and nuclear magnetic resonance measurements performed on fragments [16] are limited to the study of the arrangement of Ig domains in the *I* band of the $I_{27}I_{28}$ pair and $I_{27}I_{30}$ tetramer. The consecutive Ig domains within the pairs $I_{10}I_{11}$, $I_{27}I_{28}$, and $I_{29}I_{30}$ were studied in a complementary report by thermodynamics, cross-linking, and complexation approaches [17]. The latter study concluded that only weak

interactions between domains occur; this was later confirmed by work on a set of related fragments of two and three adjacent domains, respectively, derived from the $I_{27}I_{32}$ region [18], namely, the pairs $I_{27}I_{28}$, $I_{28}I_{29}$, $I_{29}I_{30}$, and $I_{31}I_{32}$, and the trimers $I_{29}I_{31}$ and $I_{30}I_{32}$. Recently, in the effort to clarify the structural interdomain arrangements, Marino *et al.* [19] examined the overall conformation of a six-Ig fragment $I_{65}I_{70}$. Their results, in agreement with estimations by Improta *et al.* [16], showed that this segment preferentially adopts an extended conformation in solution and exhibits a certain stiffness. However, the authors remarked that it must yet be demonstrated that these results are representative of the general *I*-band features. In fact, they suggest it should be borne in mind that Ig fragments in solution can exhibit a certain conformational heterogeneity. Extended domain pairs might be subject to bending, twisting, and tilting, according to the relative stiffness of the individual hinges.

In order to obtain a closer insight into the relationship between structure and flexibility of the fragments, a comparative study of purified β-connectin corresponding to the *A*-band part of the protein (mainly physiologically inelastic) and a fragment from the physiologically elastic *I*-band part with 100 nm contour length (the number of the domains in the fragment can be estimated to be 25, starting at the I_{20} domain) was carried out applying scattering techniques, static and dynamic light scattering and small-angle neutron scattering, as well as video particle tracking microrehology [20]. For a comparative study of the whole β-connectin and the fragment, the techniques used provide direct information on size, viscosity, and diffusion coefficient to estimate the persistence length, the gyration radius, and the hydrodynamic radius. All the results point to the flexible Gaussian chain nature of the β-connectin and its fragments. In addition, emphasizing the role of dynamic light scattering as a molecular probe of the thermal denaturation of protein in general, the authors demonstrated that β-connectin and its *I*-band fragments experience a similar thermal denaturation process, i.e., the protein unfoldes. This process involves a change in the length and hydrodynamic size of the β-connectin above a threshold temperature.

The goal of this paper is to characterize the fragments of β-connectin of the human cardiac muscle in native (folded) and denaturated (unfolded) state. These fragments belong to the *I*-band of the sarcomer and are four domains from I_{27} to I_{30} and eight domains from I_{27} to I_{34} that we name the tetramer and octamer, respectively. Each domain is composed of around 90 aminoacids. As far as we know, this study of a β-connectin octamer is the first in the scientific literature.

In this work, the use of dynamical light scattering on β-connectin fragments in solution to study the evolution of the translational diffusion coefficient and hydrodynamic radius as a function of temperature from 20 to 86 °C makes it possible to measure the size of the fragments in the native state and the size variation during thermal denaturation, with the aim of giving insight into the protein folding-unfolding process. The longer fragment, the octamer, shows a hydrodynamic size smaller than that of the tetramer in folded and unfolded states. This unexpected behavior has been interpreted in this paper to be of physical origin.

Atomic force microscopy has been shown to be an important and innovative technique to characterize proteins and to get insight into their aggregation properties [21–23]. In this work AFM images of both tetramers and octamers were obtained to study the shape of the fragments and their distributions on the substrate. In addition, in order to highlight the interactions among fragments, AFM imaging was also performed on octamers near the protein isoelectric point (IEP) and fragment aggregates were detected. These measurements were useful to complete and to confirm the scenario shown by DLS.

II. MATERIALS AND SAMPLE PREPARATION

β-connectin fragments of interest were prepared as detailed in Appendix A, and were stored at 4 °C. The preparation procedure reported in Appendix A assures that proteins in pure water are the output of the affinity chromatography procedure. Thus, the solvent (water) viscosity values at the different temperatures were taken from Ref. [27]. The tetramer and octamer fragments have molecular weights 44 and 87 kDa, respectively.

The fragment concentration was 0.096 and 0.083 mg/ml for tetramer and octamer solutions, respectively, in the DLS measurements. These solutions were filtered by Millex-GV (PVDF) Millipore filters with 0.22 μm pore size in cylindrical light scattering cells (2.5 cm inner diameter) previously cleaned and treated to be dust-free.

For AFM measurements, a 20 μl drop of 0.06 mg/ml β-connectin fragment solution was put on a freshly cleaved mica sheet and left to absorb on the surface for 5 min. After incubation, the treated surface was rinsed with deionized water to remove the excess protein and then dried under a light nitrogen flow. Furthermore, an octamer solution near the IEP was prepared with addition of hydrochloric acid (HCl) and deposited on the substrate for the AFM investigation.

III. METHODS

A. Dynamic light scattering

A description of the dynamic light scattering technique is reported in Appendix B. Quasielastic light scattering (QELS) experiments were carried out on a Brookhaven Instruments apparatus (BI 9000AT correlator and BI 200 SM goniometer). The signal was detected by an EMI 9863B/350 photomultiplier. The light source was a Coherent Innova 90 argon laser, at $\lambda = 514$ nm, linearly polarized in the vertical direction, with power attenuated in order to avoid sample heating (maximum power 100 mW). The laser long-term power stability was $\pm 0.5\%$. Homodyne detection was recorded in the angular range 15°–155° using decahydronaphthalene as cell matching liquid. The scattering angle θ was measured by the BI goniometer with resolution of 0.01°.

To calibrate the apparatus, a solution of 94 nm size latex spheres from SERVA, Standard Dow Latex, was used in the angular range 15°–155°. The data analysis of the latex solution was performed by cumulant expansion stopped at the second moment [25].

The index of refraction for both solutions at each temperature investigated by light scattering was measured using an Abbé refractometer (ATAGO 3T) with resolution of

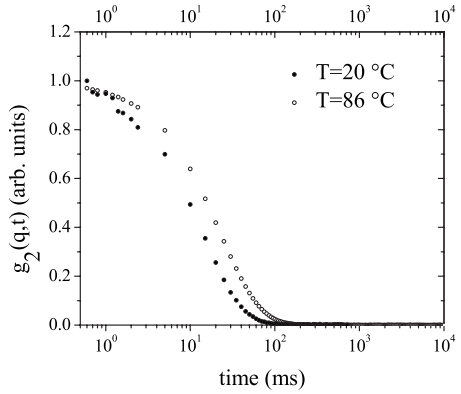

FIG. 1. DLS normalized experimental correlation functions at 90° for tetramer solutions.

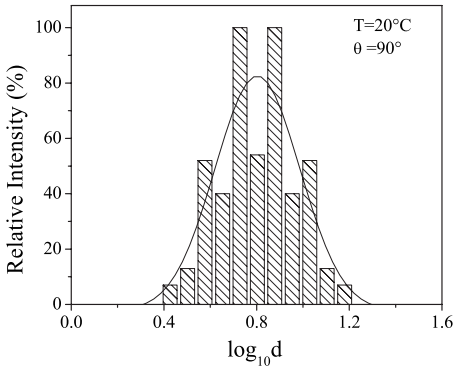

FIG. 3. Particle size distribution of tetramer solution at 20 °C at 90°. In Figs. 3–8, the histogram maximum height is normalized to 100% by intensity.

0.0001. The index of refraction of the fragment solutions at 20 °C was 1.3335 for tetramers and 1.3339 for octamers, very close to the measured water index of refraction at the same temperature, 1.3330.

The samples were thermally stabilized by a thermostat within ±0.2 °C in the thermal range studied, 20–86 °C. The sample temperature was increased step by step, ensuring that thermal stabilization was attained. Then the sample was cooled from 86 to 20 °C.

B. AFM imaging

AFM measurements were performed using a PicoSPM microscope equipped with an AAC-mode controller (Molecular Imaging, Phoenix, AZ). The AFM images were acquired in intermittent contact mode using a rectangular supersharp silicon noncontact cantilever (model SSS-NCH, NanoWorld AG, Switzerland) with 330 kHz typical resonance frequency. Scan rate was 0.2 lines/s. In particular, AFM images of octamers near the IEP were performed in contact mode in PBS buffer and using a rectangular silicon contact cantilever (model CSG01, NT-MDT & Co., Moscow, Russia) with a spring constant of 0.03 N/m. Scanner calibration was periodically checked by means of a reference grid (TGZ02 from MikroMash, Tallin, Estonia). All the experiments were performed at room temperature. AFM images of 500×500 nm^2 (512×512 pixels) were processed with standard flattening procedures.

IV. RESULTS

A. Dynamic light scattering

QELS experiments were performed on tetramers and octamers in solutions at 20 °C for several scattering angles from 15° to 155° and, at fixed angles, as a function of temperature from 20 to 86 °C. The data analysis reported in this paper is performed on samples having concentrations of 0.096 mg/ml for tetramers and 0.083 mg/ml for octamers in aqueous solution. However, double concentrations for both fragments were also measured at 20 °C to exclude interactions among fragments. The sizes found for the more concentrated samples were the same as for the less concentrated ones; thus at these concentrations the particle interactions are negligible.

For both tetramer and octamer solutions, the cumulant analysis was not employed because no good residuals were found, residuals being the differences between experimental and fitted curves. On the contrary, good residuals $\leq 1\%$ were obtained by the CONTIN analysis. One or more populations with broad size distribution were detected.

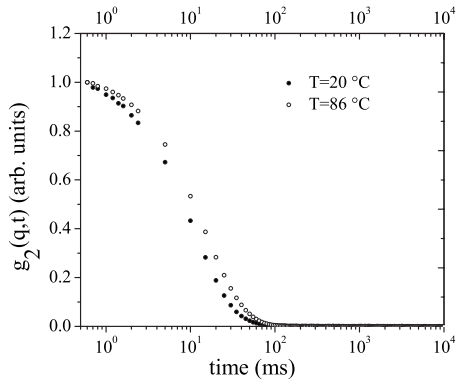

FIG. 2. DLS normalized experimental correlation functions at 90° for octamer solutions.

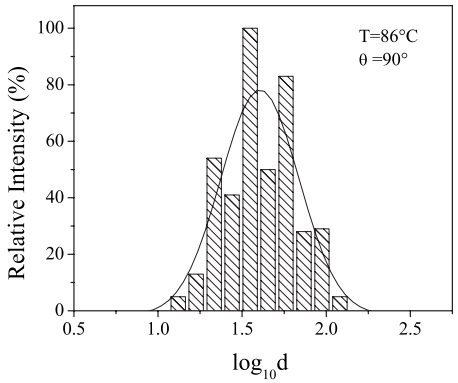

FIG. 4. Particle size distribution of tetramer solution at 86 °C at 90°.

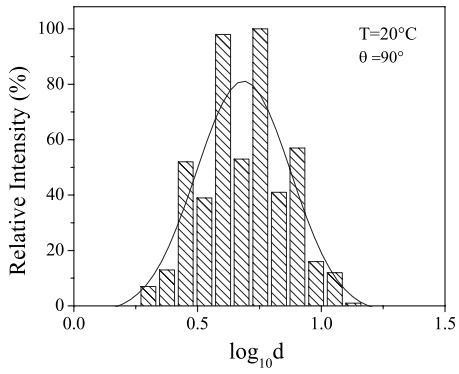

FIG. 5. Particle size distribution of octamer solutions at 20 °C at 90°.

Figures 1 and 2 show the autocorrelation functions at $\theta = 90°$ for both solutions, at the temperatures of 20 and 86 °C in identical experimental conditions. For all the curves the measured baselines were subtracted. The decay of the autocorrelation function moves to larger times as the temperature increases, indicating an increase of the fragment sizes. In Figs. 3–6 are reported some CONTIN histograms of the size distribution related to measurements that show a single population at $\theta = 90°$, for both 20 and 86 °C. The size distribution covers one order of magnitude; no smoothing was used for the histograms. The increase of the size, due to temperature increase, is quite important and suggests a transition from the folded to the unfolded state. In fact, the thermal denaturation breaks the secondary and tertiary structures of the fragments, and thus the filament (random coil) occupies a larger spatial region. In addition, in Figs. 7 and 8, CONTIN histograms of tetramer and octamer solutions at $\theta = 20°$ and $T = 20$ °C are shown to detect the possible presence of larger structures. Two populations can be observed for both solutions. The small-size population corresponds to fragments in the folded state (see figure insets) whereas the other populations are aggregates, i.e., clusters, of fragments. The latter populations are very small.

In Table I, the size distribution for measurements at two angles, 90° and 15°, for 20, 40, 60, 80, and 86 °C is reported. The percentage of the population (by intensity) is also reported to give an insight into the fragment aggregation phenomenon [28]. Of note, for both fragments, the second population corresponding to the aggregates is observed only at small angles, whereas at $\theta = 90°$ a single population is detected from 20 to 86 °C. This signifies that the sample is mainly composed of fragments in solution and the fragments in solution scarcely aggregate. In Table I are also reported the size distributions and percentages of the populations at 20 °C after denaturation for both fragments. For tetramers at $\theta = 90°$ only one population can be observed from 20 to 86 °C. The maximum diameter of the histograms increases from 15 nm at 20 °C up to 43 nm at 60 °C and increases further up to 121 nm at 86 °C; then it remains the same at 20 °C after denaturation. At $\theta = 15°$, two populations were always observed. The smaller objects show a maximum diameter of 13 nm at 20 °C that increases up to 29 nm at 60 °C and up to 75 nm at 86 °C. At the last temperature, three different populations were detected. Coming back to 20 °C

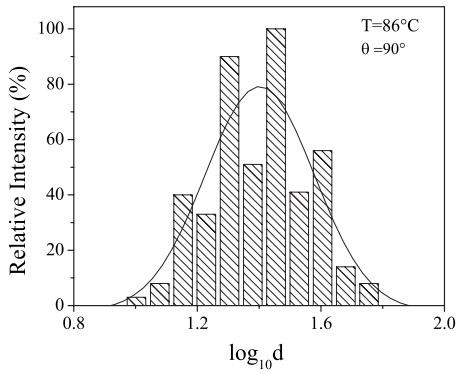

FIG. 6. Particle size distribution of octamer solutions at 86 °C at 90°.

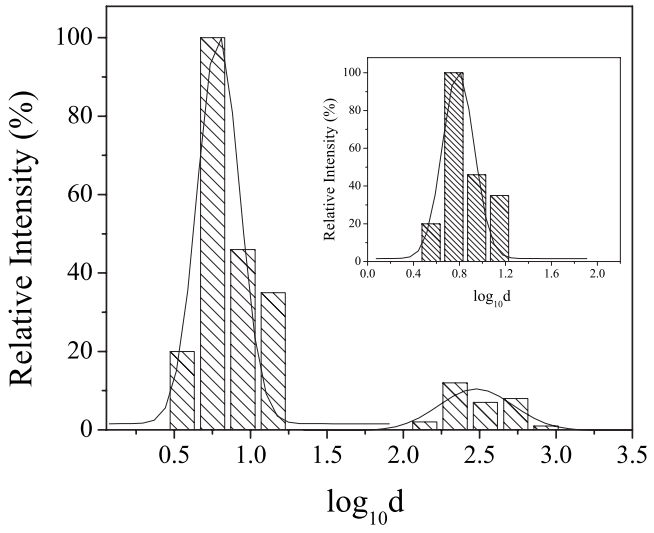

FIG. 7. Two populations, tetramers and aggregates, are shown at 20 °C and 20°. In the inset the fragment population is reported.

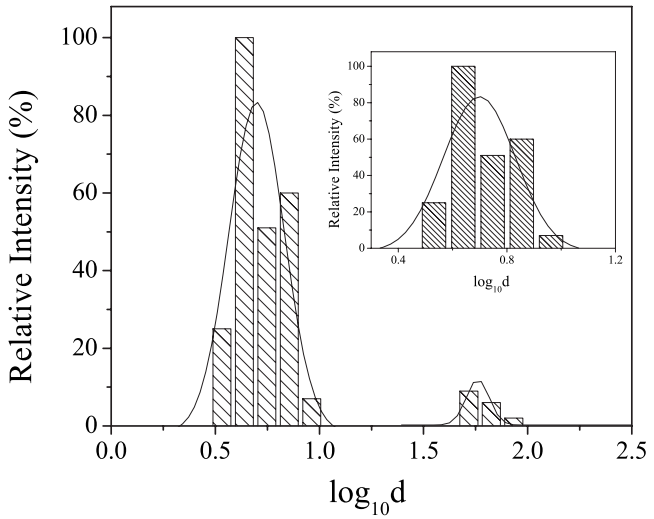

FIG. 8. Two populations, octamers and aggregates, are shown at 20 °C and 20°. In the inset the fragment population is reported.

TABLE I. Distribution of the hydrodynamic diameters d and d_a and respective population percentages (by intensity) over total for both fragments in solutions and aggregates of the fragments as a function of temperature.

		Tetramer				Octamer			
T (°C)	θ	d (nm)	%	d_a (nm)	%	d (nm)	%	d_a (nm)	%
20	90°	2.7–15	100			2.0–13	100		
	15°	4.2–13	91	68–119	9	3.6–8.3	91	158–242	9
40	90°	1.5–24	100			1.2–14	100		
	15°	4.1–14	90	174–609	10	2.5–11	92	44–79	8
60	90°	3.1–43	100			1.9–23	100		
	15°	4.4–29	93	313–808	7	3.8–9.2	56	12–28	44
80	90°					1.4–5.9	8	14–33	92
	15°					12–33	93	1075–1770	7
86	90°	13–121	100			2.9–6.2	3	13–46	97
	15°	24–75	46	242–526	23				
	15°			1686–5400	31				
20[a]	90°	14–110	100			9.0–82	100		
	15°	35–144	37	595–1211	38	14–55	20	403–5800	80
	15°			10200–42150	25				

[a]Values at 20 °C after thermal denaturation.

after denaturation, the maximum d value is 144 nm, greater than the value, 75 nm, at 86 °C. In the thermal range 20–60 °C, aggregates of maximum diameter varying from 119 to 808 nm were detected (see Table I); this population is ~10% of the total. At 86 and 20 °C after denaturation, three populations were observed. At 86 °C the smallest population, described above, is compatible with the denaturation of fragments, whereas a second population of fragment aggregates of maximum diameter 526 nm is observed and a third population of greater fragment aggregates (maximum diameter 5400 nm) was also found. The percentages of these populations are 46%, 23%, and 31% for small-, medium-, and large-size populations, respectively. Also, for aggregates, larger sizes were detected at 20 °C after denaturation. Of note, once the aggregation process starts it gives larger and larger aggregates vs time. Similar results were found for octamers (see Table I).

We now focus our attention on the fragment population. The autocorrelation functions were detected and Γ values were measured. Several measurements for each angle were performed to calculate the angular average, Γ_{av}. The latter was found proportional to q^2 in the angular range investigated. This trend was observed for all the temperatures studied. This result shows that, for both fragments, the process studied is diffusive at each temperature, and the diffusion coefficient D is the translational one. In Fig. 9, the calculated translational diffusion coefficient D of both fragments is reported as a function of the scattering angles. In the limit of the experimental errors, $D(\theta)$ is constant; thus it is possible to give angular averaged values, reported in Table II for both fragments. The error reported in Table II is the standard deviation σ of the averages. The fragment hydrodynamic diameters d have been calculated by the Stokes-Einstein equation and are reported in Table II. In Fig. 10 $D(\theta)$ is reported for both denatured fragment populations. Because of the averaging process over the whole angular range, the precision of the D and d values for each temperature increased. In Table II, D increases as a function of the temperature increase up to

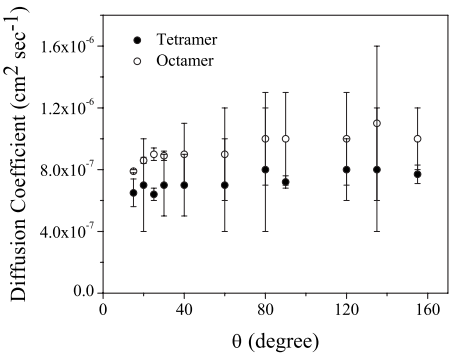

FIG. 9. Translational diffusion coefficient of the fragment population in the whole angular range at 20 °C.

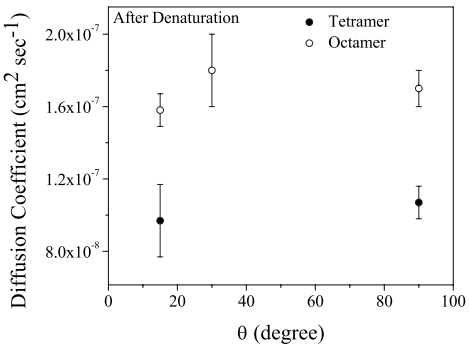

FIG. 10. Translational diffusion coefficient of the fragment population at 20 °C, after thermal denaturation.

TABLE II. Index of refraction, translational diffusion coefficient, and diameter of the fragments in solution as a function of temperature.

	Tetramer			Octamer		
T (°C)	n	D (10^{-7} cm^2/s)	d (nm)	n	D (10^{-7} cm^2/s)	d (nm)
20	1.3335	6.9 ± 0.2	6.1 ± 0.2	1.3339	8 ± 0.1	5.18 ± 0.07
30	1.3328	8 ± 2	7 ± 1	1.3334	10 ± 1	5.3 ± 0.7
40	1.3314	10.7 ± 0.5	6.4 ± 0.3	1.3325	15 ± 3	4.7 ± 0.8
50	1.3300	10.9 ± 0.8	7.9 ± 0.6	1.3305	17 ± 3	5.0 ± 0.8
60	1.3278	9.6 ± 0.7	10.7 ± 0.8	1.3284	16 ± 2	6.3 ± 0.8
70	1.3258	5.4 ± 0.1	20.9 ± 0.5	1.3260	8.9 ± 0.7	14 ± 1
80	1.3238			1.3238	6.5 ± 0.3	22 ± 1
86	1.3226	4.4 ± 0.5	36 ± 4	1.3225	7 ± 1	24 ± 4
20[a]	1.3335	1.05 ± 0.08	40 ± 3	1.3339	1.67 ± 0.06	25.2 ± 0.9

[a]Values at 20 °C after thermal denaturation.

a maximum at 50 °C and decreases for a further temperature increase, whereas d increases sharply above 50 °C.

In summary, for tetramers, the hydrodynamic diameter is 6.1 ± 0.2 nm at 20 °C and increases to 36 ± 4 nm at 86 °C; for octamers it is 5.18 ± 0.07 nm and increases to 24 ± 4 nm at 86 °C. After denaturation, at 20 °C both fragments maintain the denatured size; thus denaturation is not reversible over the whole thermal range. Of note, the octamer size is smaller than the tetramer size in both native and denatured states, whereas the octamer contour length is twice the tetramer one.

B. AFM imaging

Even though fragments and their aggregates in solution can differ from adsorbed fragments and aggregates on a substrate, AFM images were very useful to confirm some DLS results. In Fig. 11 representative AFM images of tetramers and octamers in the native state deposited on a mica substrate are shown. A homogeneous and uniform distribution of comparable structures with a quasiellipsoidal shape can be observed. Reproducible images were acquired on different regions of the samples, suggesting the homogeneity of the solution deposited. A quasiellipsoidal shape for both tetramers and octamers is observed. A line profile of each feature was performed. In particular, the length and width, corresponding, respectively, to major and minor axes, were evaluated. The analysis was performed on 500×500 nm^2 images. Histograms of the length and width distributions are shown in Figs. 12–15. The tetramers show a mean value (averaged over 100 structures) length of 25.5 ± 1.9 nm, and a mean value width of 20.2 ± 1.7 nm, and octamers have a mean value length of 21.3 ± 2.1 nm, and a mean value width of 17.9 ± 1.9 nm. All measurements are expressed with their standard deviations. Despite the typical broadening of lateral size in AFM measurements due to the tip-probe geometry, the octamers are smaller than the tetramers, in agreement with the DLS results.

In order to highlight the mechanism of aggregation of the fragments, AFM imaging of octamers near the IEP (the condition at which proteins carry no net charge) was performed (see Appendix A for details). When the fragments have no charge, their aggregation is favored because the balance between repulsion and attraction fails, the repulsive interaction component being strongly reduced. In consequence of HCl addition, we expected a modification in the packing of the

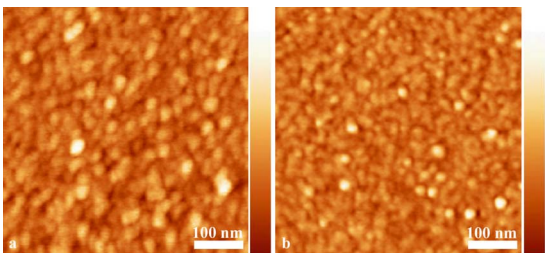

FIG. 11. (Color online) AFM images of (a) tetramer and (b) octamer fragments deposited on mica substrate. Image size is 500×500 nm^2. Z (vertical) ranges are 4.0 (a) and 4.1 (b) nm.

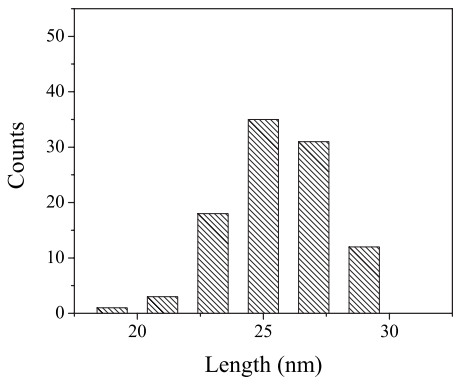

FIG. 12. Histograms of length distribution for tetramers. For each histogram of Figs. 12–15, 17, and 18, 100 structures have been analyzed. The numerical counts represent how many structures with the size reported on the abscissa have been counted.

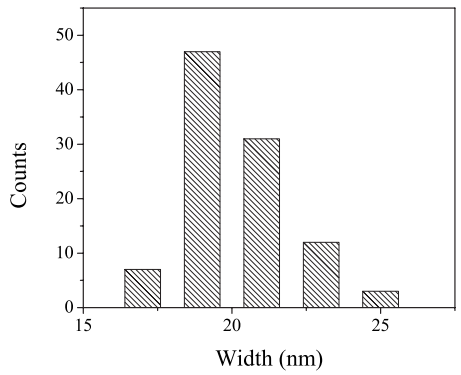

FIG. 13. Histograms of width distribution for tetramers.

protein with respect to the native structure, and moreover an aggregation trend. In fact, in Fig. 16(a), where a representative AFM image is shown, a carpet of homogeneous fragments can be observed. These structures maintain an ellipsoidal shape though more elongated. From the line profile analysis, performed on a 500×500 nm^2 image, the fragments show a mean value length of 34.3 ± 3.4 nm, and a mean value width of 24.4 ± 3.7 nm. All measurements are expressed with their standard deviations. Histograms of the length and width distributions are shown in Figs. 17 and 18. These structures are bigger than the native ones (see histograms of Fig. 13), suggesting an initial unfolding due to HCl addition.

In the image, above this fragment distribution, it is also possible to observe two different and isolated structures. A more detailed analysis suggests that these structures are generated by successive layers of fragments. In particular, it is possible to resolve their inner structure, composed of subunits whose lateral size is comparable with that of the octamers underneath. Moreover, the line profiles of Figs. 16(c) and 16(d) in both structures show a step height, with respect to the background, of about 6 nm. Whereas the resolution in the lateral size is poor (several nanometers) due to the convolution of the tip, the vertical resolution is 1 nm, since it is not affected by the size of the probe. Thus the step measurement is in quantitative agreement with the octamer size at the intermediate state of thermal denaturation at 60 °C (see Table II). Furthermore, AFM images give a confirmation of the presence of aggregates in a different condition from that of the fragments in solution, i.e., on the substrate, and detect the shape of fragments and aggregates. The profiles of Figs. 16(c) and 16(d) give lateral sizes of the aggregates of 400 and 200 nm, respectively, similar to the DLS sizes.

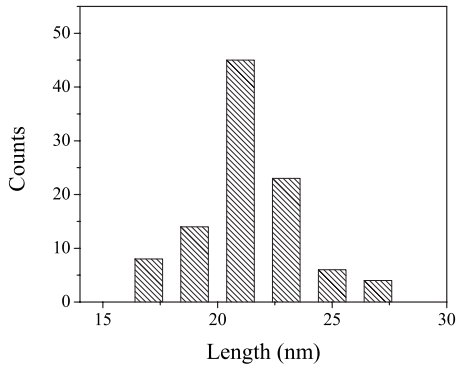

FIG. 14. Histograms of length distribution for octamers.

V. DISCUSSION

The size of both fragments was measured by DLS in the whole thermal range and thermal denaturation was found to be irreversible. The fragment sizes increase with temperature. The native and denatured sizes are smaller for the octamer although its contour length is twice the tetramer one. This result will be the subject of further investigation; one hypothesis concerns the significance of hydrophobic interactions between domains of the given fragment. In addition, AFM imaging provides information on the shape of the fragments, quasiellipsoidal for native and denatured states, with a more ellipsoidal shape for unfolded fragments. Quite interestingly, fragment aggregates have also been detected by DLS and AFM in particular conditions, i.e., at high temperature or at the protein isoelectric point, with comparable sizes of 200–400 nm. See Table I and Figs. 14(c) and 14(d). By AFM the important information was obtained that the aggregate is composed of fragments that are close to each other. Thus adhesion forces play the main role, the protein charge being zero at the IEP.

In order to investigate the overall domain arrangements and their temperature dependence in our *I*-band Ig fragments (tetramers and octamers), we compare the results from the current study, DLS and AFM imaging, with literature data. In the frame of available models, the wormlike chain model is most commonly applied to β-connectin filaments to describe its conformation [4,29]. In this description, β-connectin behaves as a polymer and tandem Ig domains may therefore be pictured as a necklace of independent beads in a rather extended conformation, connected by stiff hinges. It should be noted that the WLC model is generally used for polymers with contour length much longer than the bond length and an infinite number of bonds. However, for Ig fragments with a limited number of domains like ours, this model is not suitable and, as reported in the literature in similar cases [19,20], we apply the flexible Gaussian chain model of Rouse and Zimm [30] to describe these fragments. A Gaussian coil is modeled as a collection of beads. N Gaussian segments, each of average length b, are connected by $N+1$ identical beads [30]. The segments are assumed to provide Hookean restoring forces to the beads. The contour length of the coil is given by $L=Nb$, and its mean-square end-to-end distance is given by $\langle R^2 \rangle = Nb^2 = Lb$. The theoretical calculation for a flexible Gaussian chain in a θ solvent gives the expected value of $R_g/R_H = 8/(3\sqrt{\pi}) = 1.50$ from Zimm theory [30]. We start with the tetramer, whose Stokes radius is $R_H = 3.05$ nm at 20 °C in the native state (see Table II). On the other hand, the value of the radius of gyration from SAXS data [16] was estimated to be $R_g = 4.54$ nm. Combining these two results, we obtain the ratio between the radius of gyration and the hydrodynamic size, $R_g/R_H = 1.49$, in agreement with the accepted theoretical value and with modern molecular dynamics simulations [31]. Since the estimation of the

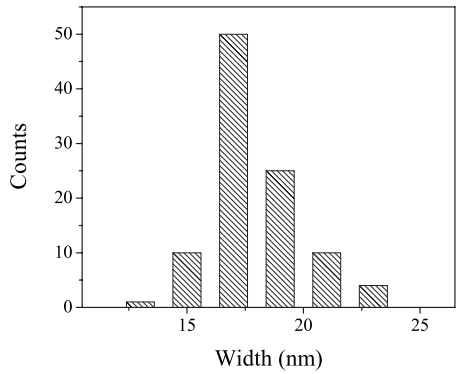

FIG. 15. Histograms of width distribution for octamers.

Stokes radius from the observed diffusion coefficient value is model independent (coil or rod), the ratio 1.49 assures that the present analysis can be based on Gaussian coils and provides additional proof of the flexible Gaussian nature of the fragment. A similar calculation cannot be carried out for the octamer because, until now, its radius of gyration has not yet been reported in the literature. However, from our scattering data on the octamer (Table II) we estimated a Stokes radius of R_H=2.59 nm at 20 °C (native state). Of note, this value is 15% shorter than the tetramer R_H. Although lateral size measurements with the AFM are limited by the probe geometry, and direct quantitative comparison between AFM and DLS numerical results is not appropriate, AFM measurements confirm a dimensional decrease (length 16% and width 11%) from tetramer to octamer. The smaller octamer size can be explained by taking into account that the longer the length of the fragment the greater can be the torsional modes of rotation and hydrophilic or hydrophobic interdomain interactions [32,33]. Recently, the crystal structure of a three-Ig apical fragment [34] shows a slightly bent conformation in which domains 1 and 2 are arranged in a linear fashion but domain 3 is tilted with respect to its adjacent domain. In addition to these linear arrays, crystal structures of four-Ig segments from the neural cell adhesion molecule axonin-1 or TAG-1 [35] and the lipopolysacccharide-binding immune protein hemolin [36] exhibit compact, U-shaped arrangements due to contacts between domains 1 and 4 and 2 and 3 in the molecule. These examples illustrate the diverse means by which multi-Ig proteins achieve specific conformations, like ours. By comparison, it thus appears that degree of bending and twisting of the domains with respect to each other in the fragment of eight domains results in an overall shortening in their size compared with the four-domain fragment.

In addition, we compare the hydrodynamic size of the tetramer and octamer during and after thermal denaturation. To date, in the recent report [20] cited in the introduction, Di Cola *et al.* showed the heat-induced unfolding of the whole β-connectin and its fragment. The authors observed that the temperature increase between 25 and 45 °C causes a gradual unwinding with small changes in size, followed by a sharp change over 60 °C. A similar trend, in the same thermal range, comes from the temperature dependence of the hydrodynamic diameter by our DLS data for both fragments. The increase of the hydrodynamic diameters of the fragments is an obvious consequence of the unfolding that occurs as temperature is increased. Several bonds in the fragments are first weakened and then broken. As heating continues, some of the hydrogen bonds that stabilize the structure will begin to break. So the protein obtains a more flexible structure and

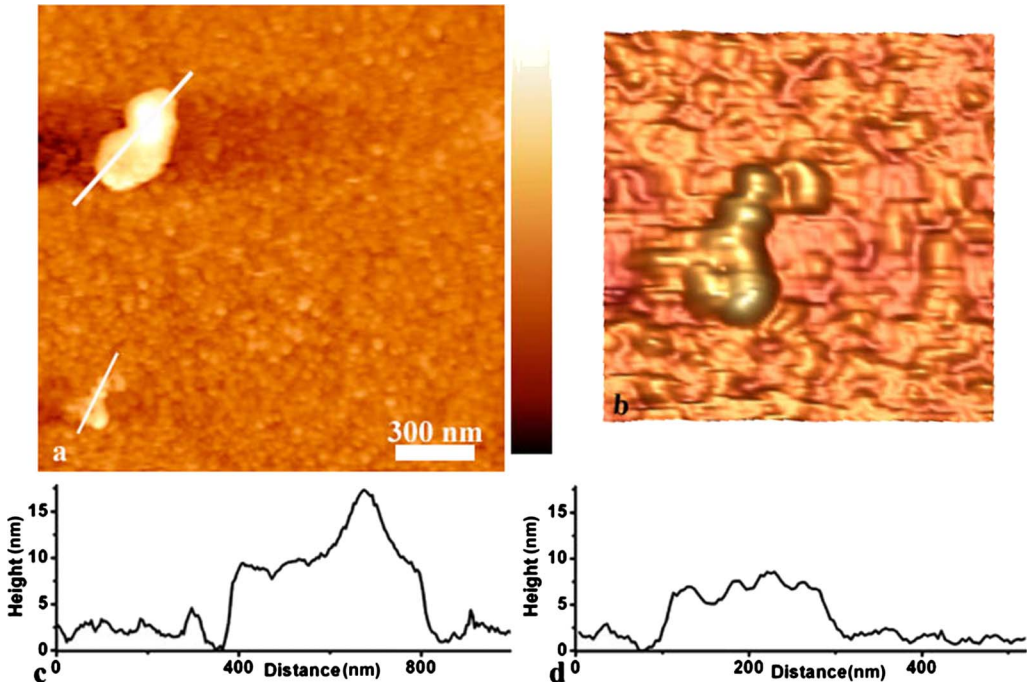

FIG. 16. (Color online) (a) AFM image of octamer fragments near isoelectric point. Image size is 1.8×1.8 μm^2. Z range is 23.7 nm. Two isolated aggregates of octamers are observable. (b) Three-dimensional zoom of image (a) on the smaller aggregate. (c), (d) Line profiles along big (c) and small (d) aggregates showing the protein height.

some hydrophobic groups, buried inside the compacted native structure, became exposed to solvent. The hydrophobic group exposure increases the amount of water bound by the protein and the hydrodynamic size. Moreover, because the exposure of this large number of hydrophobic groups to the solvent is energetically unstable, some denatured proteins aggregate with each other, minimizing the interaction with water. In fact, three different populations are observed at 86 °C for both the tetramer and the octamer, one corresponding to the denatured state and the other two to the aggregate state. Upon cooling, any attempt to obtain the native structure would first require that the hydrophobic bonds be broken. This process, energetically unfavorable and highly unlikely, prevents the return to the native state. The comparison of the fragments' hydrodynamic diameters between 86 and 20 °C after denaturation is in agreement with this scenario and confirms, therefore, that the protein fragments cannot revert to their original condition and the process is accordingly irreversible.

In order to better investigate the aggregation properties of the protein fragments we obtained AFM images on octamers near the isoelectric point. The *p*H change induced by HCl addition alters the charge distribution on the protein surface. As a consequence of the electrical neutralization, the hydrophobic packing is reduced and a slight increase of lateral size of each fragment is observed. At the same time, the reduction of surface charge favors fragment-fragment aggregation. As observed in the AFM measurements, this process is carried out by the combination of subunits, probably driven by hydrophobicity effects as earlier reported [22]. Moreover, this coexistence of fragments and aggregates in the denatured state is in agreement with the population distribution found in the analysis of DLS data.

VI. CONCLUSION

DLS and AFM imaging methods were used to study two fragments of β-connectin, the tetramer $I_{27}I_{30}$ and the octamer $I_{27}I_{34}$ of the sarcomer *I* band. DLS provides the size of both fragments as a function of temperature from 20 up to 86 °C. A thermal denaturation on temperature increase is shown for both fragments. For the tetramer the hydrodynamic diameter of 6.1 nm at 20 °C increases up to 36 nm at 86 °C and for the octamer the increase is from 5.18 to 24 nm in the same thermal interval. The octamer is smaller than the tetramer in both folded and unfolded states even though the contour length of the octamer is twice that of the tetramer. This feature seems related to the significance of hydrophobic interactions between domains of a given fragment. The longer the fragment, the more easily the hydrophobic parts of the domains interact with each other. Furthermore, fragment aggregates were detected by both techniques. Of note, the aggregate increase follows the temperature increase which leads, as reported above, to a size increase due to unfolding. Thus protein unfolding and protein aggregation are parallel processes. By AFM the aggregates were found to be composed of partially unfolded fragments very close to each other. In our opinion, the adhesion forces, mainly hydrophobic, play the main role in this aggregation, since at the isoelectric point the protein has zero charge.

ACKNOWLEDGMENTS

We thank R. Livi, L. Casetti, and C. Guardiani for helpful seminars and discussions. This work was supported by Italian MUR, PRIN2005, and INFM. We thank Strep EU Project No. 12835 EMBIO ("Emergent Organization in Complex Biomolecular Systems") for support. Thanks are also due to Ente Cassa di Risparmio di Firenze for funds.

APPENDIX A

β-connectin fragments were amplified by reverse transcription and polymerase chain reaction (RTPCR) from 1 μg of human cardiac total RNA using the SuperScript one-step RT-PCR kit (Invitrogen, Milan, Italy), according to the manufacturer's instructions. The PCR primers flanking the $I_{27}I_{30}$ and $I_{27}I_{34}$ fragments were designed according to the published human cardiac β-connectin cDNA sequence (GenBank accession number X90568) in order to obtain a COOH-terminal Cys^2 tag for immobilization on solid surfaces. The PCR products of the expected sizes 1076 base pairs (bp) for the $I_{27}I_{30}$ and 2144 bp for the $I_{27}I_{34}$ fragments were identified by agarose gel electrophoresis and then cloned into the Champion pET 100 Directional TOPO vector (Invitrogen,

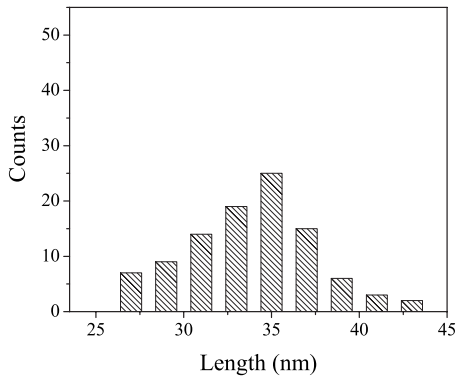

FIG. 17. Histograms of length distribution for octamers near isoelectric point.

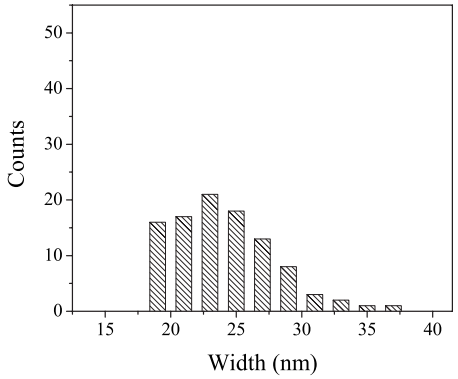

FIG. 18. Histograms of width distribution for octamers near isoelectric point.

Milan, Italy), fused with an NH_2-terminal His^6 tag for fragment purification. The identity of the cloned fragments was verified by DNA sequencing with the use of a standard automated sequencer. Expression of the fragments was induced in BL21(DE)3 cells by 0.1 m*M* isopropyl-β-D-thio-glactopyranoside (IPTG) at 37 °C for 4 h. The proteins were expressed in soluble form and were purified by Ni affinity chromatography (Novagen, Milan, Italy), according to the protocol provided by the manufacturer. Fusion proteins were eluted in buffer solution of 50 m*M* Tris-HCl, 0.5 m*M* NaCl, and 80 mM ethylene diamine tetra-acetic acid with pH=8 and Debye screening length 0.41 nm. It is notable that the pH of these protein solutions is 7.34 measured by Metrohm glass electrode PH-207. This value is higher than pH=5.80, the isoelectric point of the protein, calculated using the ExPAsy Proteomics server [37]. The IEP is the pH at which a protein carries no net charge.

Given the variations of the synthesis procedure, we decided to check the sample before each measurement, performing one test by dielectric spectroscopy to verify the reproducibility of the specimen. In fact, the biological procedure is long and made up of several steps. Dielectric spectra of the buffer solution and of both fragments in solution were measured in the frequency range 0.5–50 GHz using an Agilent N5230A vector network analyzer. From the comparison of these spectra with the water spectrum in the same frequency range, it is possible to have a fast and accurate verification of the sample reproducibility.

APPENDIX B

In the dynamic light scattering technique, the normalized time autocorrelation function $g_2(q,t)$ of the scattered light intensity $I(q,t)$ is measured:

$$g_2(q,t) = \frac{\langle I(q,0)I(q,t)\rangle}{\langle I(q,0)^2\rangle}.$$

The latter can be expressed in terms of the field autocorrelation function $g_1(q,t)$ through the Siegert equation [24]

$$g_2(q,t) = A[1 + \beta|g_1(q,t)^2|],$$

where A is the $g_2(q,t)$ background and β is the coherence factor [25]. $g_2(q,t)$ will be named the autocorrelation function in this paper. For the fragments in solution, the measured autocorrelation functions were analyzed by CONTIN, a constrained regularization method for determining size distributions, especially suitable for samples with a broad population or for samples with more than one population [25,26]. The buffer solution without fragments was also measured and analyzed by the cumulant method. CONTIN did not converge in this case. A diameter of 0.04 nm with polydispersity of 2% was found; thus no particles were in the buffer solution and the signal was due to the photomultiplier dark count autocorrelation function. This fast decay was excluded by measurements on fragments in solution, for all the measurements.

Once Γ of the autocorrelation function is known, i.e., the inverse relaxation time of the given process, the average diffusion coefficient D is related to Γ by

$$D = \Gamma/q^2,$$

where $q=(4\pi n/\lambda)\sin(\theta/2)$ is the scattering wave vector, n is the index of refraction of the sample, and θ is the scattering angle. When D is the fragment translational diffusion coefficient, it is related to the hydrodynamic diameter $d=2R_H$ (where R_H is the hydrodynamic radius of the fragment) through the Stokes-Einstein relationship:

$$D = k_B T/(6\pi\eta R_H),$$

where $k_B T$ is the thermal energy and η is the viscosity of the solvent, i.e., water.

[1] A. W. Linke and H. Granzier, Biophys. J. **75**, 2613 (1998).
[2] A. W. Linke, M. R. Stockmeier, M. Ivemeyer, H. Hosser, and P. Mundel, J. Cell Sci. **111**, 1567 (1998).
[3] K. Maruyama, Int. Rev. Cytol. **104**, 81 (1986).
[4] H. Higuchi, Y. Nakauchi, K. Maruyama, and S. Fujme, Biophys. J. **65**, 1906 (1993).
[5] M. Rief, M. Gautel, F. Oesterhelt, J. M. Fernandez, and H. E. Gaub, Science **276**, 1109 (1997).
[6] L. Tskhovrebova and J. Trinick, J. Mol. Biol. **265**, 100 (1997).
[7] L. Tskhovrebova and J. Trinick, J. Mol. Biol. **310**, 755 (2001).
[8] M. S. Kellermayer, S. B. Smith, H. L. Granzier, and C. Bustamante, Science **276**, 1112 (1997).
[9] L. Tskhovrebova, J. Trinick, J. A. Sleep, and R. M. Simmons, Nature (London) **387**, 308 (1997).
[10] H. Li, W. A. Linke, A. F. Oberhauser, M. Carrion-Vazquez, J. G. Kerkvliet, H. Lu, P. E. Marszalek, and J. M. Fernandez, Nature (London) **418**, 998 (2002).
[11] K. Watanabe, C. Muhle-Goll, M. S. Kellermayer, S. Labeit, and H. Granzier, J. Struct. Biol. **137**, 248 (2002).
[12] O. Mayans, J. Wuerges, S. Canela, M. Gautel, and M. Wilmanns, Structure **9**, 331 (2001).
[13] S. Improta, A. S. Politou, and A. Pastore, Structure **4**, 323 (1996).
[14] P. Bork, L. Holm, and C. Sander, J. Mol. Biol. **242**, 309 (1994).
[15] Y. Harpaz and C. Chothia, J. Mol. Biol. **238**, 528 (1994).
[16] S. Improta, J. K. Krueger, M. Gautel, R. A. Atkinson, J. F. Lefevre, S. Moulton, J. Trewhella, and A. Pastore, J. Mol. Biol. **284**, 761 (1998).
[17] A. S. Politou, M. Gautel, S. Improta, L. Vangelista, and A. Pastore, J. Mol. Biol. **255**, 604 (1996).
[18] K. A. Scott, A. Steward, S. B. Fowler, and J. Clarke, J. Mol. Biol. **315**, 819 (2002).
[19] M. Marino, D. I. Svergun, L. Kreplak, P. V. Konarev, B. Maco, D. Labeit, and O. Mayans, J. Muscle Res. Cell Motil. **26**, 355 (2006).
[20] E. Di Cola, T. A. Waigh, J. Trinick, L. Tskhovrebova, A. Houmeida, W. Pyckhout-Hintzen, and C. Dewhurst, Biophys.

J. **88**, 4095 (2005).
[21] M. S. Z. Kellermayer, C. Bustamante, and H. L. Granzier, Biochim. Biophys. Acta **1604**, 105 (2003).
[22] F. Sbrana, L. Bongini, G. Cappugi, L. Carresi, D. Fanelli, A. Guarino, B. Pantera, L. Pazzagli, B. Tiribilli, M. Vassalli, and C. Zoppi, Eur. Biophys. J. **36**, 727 (2007).
[23] R. Flamia, P. A. Zhdan, M. Martino, J. E. Castle, and A. M. Tamburro, Biomacromolecules **5**, 1511 (2004).
[24] B. J. Berne and R. Pecora, *Dynamic Light Scattering* (Dover, New York, 2000).
[25] *Dynamic Light Scattering—The Method and Some Applications*, edited by W. Brown (Oxford Science Publications, Oxford, 1993), p. 177.
[26] S. W. Provencher, Comput. Phys. Commun. **27**, 213 (1982).
[27] *CRC Handbook of Chemistry and Physics*, 70th ed., edited by R. C. Weast,D. R. Lide,M. J. Astle, and W. H. Beyer (CRC, Boca Raton, FL, 1989).
[28] S. Matysiak and C. Clementi, J. Mol. Biol. **363**, 297 (2006).
[29] L. R. G. Treloar, *The Physics of Rubber Elasticity* (Clarendon, Oxford, 1975), p. 776.
[30] H. Yamakawa, *Modern Theory of Polymer Solutions* (Harper and Row, New York, 1971), p. 419.
[31] Y. Oono, J. Chem. Phys. **79**, 4629 (1983).
[32] C. R. Cantor and P. R. Schimmel, *Biophysical Chemistry. Part III. The Behavior of Biological Macromolecules* (Freeman, San Francisco, 1980).
[33] C. S. Lai, C. E. Wolff, D. Novello, L. Griffone, C. Cuiberti, F. Molina, and M. Rocco, J. Mol. Biol. **230**, 625 (1993).
[34] V. Soroka *et al.*, Structure **11**, 1291 (2003).
[35] J. Freigang, K. Proba, L. Leder, K. Diederichs, P. Sonderegger, and W. Welte, Cell **101**, 425 (2000).
[36] X. D. Su, L. N. Gastinel, D. E. Vaughn, I. Faye, P. Poon, and P. J. Bjorkman, Science **281**, 991 (1998).
[37] www.expasi.ch